Annals of Nuclear Medicine (2018) 32:474–484
https://doi.org/10.1007/s12149-018-1270-z

ORIGINAL ARTICLE

Reconstruction/segmentation of attenuation map in TOF-PET based on mixture models

Hamidreza Hemmati[1] · Alireza Kamali-Asl[1] · Pardis Ghafarian[2,3] · Mohammad Reza Ay[4,5]

Received: 26 February 2018 / Accepted: 12 June 2018 / Published online: 21 June 2018
© The Japanese Society of Nuclear Medicine 2018

Abstract

Attenuation correction is known as a necessary step in positron emission tomography (PET) system to have accurate and quantitative activity images. Emission-based method is known as a promising approach for attenuation map estimation on TOF-PET scanners. The proposed method in this study imposes additional histogram-based information as a mixture model prior on the emission-based approach using maximum a posteriori (MAP) framework to improve its performance and make such a nearly segmented attenuation map. To eliminate misclassification of histogram modeling, a Median root prior is incorporated on the proposed approach to reduce the noise between neighbor voxels and encourage spatial smoothness in the reconstructed attenuation map. The joint-MAP optimization is carried out as an iterative approach wherein an alteration of the activity and attenuation updates is followed by a mixture decomposition of the attenuation map histogram. Also, the proposed method can segment attenuation map during the reconstruction. The evaluation of the proposed method on the numerical, simulation and real contexts indicate that the presented method has the potential to be used as a stand-alone method or even combined with other methods for attenuation correction on PET/MR systems.

Keywords TOF emission data · Reconstruction · Attenuation map · Mixture models · PET/MR

Introduction

Accurate quantification of the radiotracer activity distribution in positron emission tomography (PET) mandates the use of the approaches for attenuation correction. In combined PET/MR imaging, attenuation correction is a major challenge since direct conversion of the MR information into corresponding PET attenuation coefficients is not possible. The standard MR-based approach (MRAC) performs a segmentation into several tissue classes but neglects bone attenuation and, therefore, leads to an underestimation of the reconstructed PET activity distribution by up to 30% [1]. Moreover, the attenuation coefficients assigned to different classes are not patient-specific and may cause error especially for lungs [2]. Different methods have been proposed to overcome the attenuation correction challenges on PET/MR system that can be categorized into the atlas-based methods [3], use of special MR sequences [4, 5], partial or full transmission-based and emission-based methods [6]. The last methods tend to retrieve the attenuation coefficients from PET emission data and allow acquisition of the true 511-keV attenuation coefficients without need for conversion. These approaches attempt to derive quantitative attenuation coefficients based on the different techniques including segmentation of the uncorrected emission images into regions of approximately constant attenuation [7], applying consistency conditions for attenuation and activity maps and simultaneous reconstructions of the activity and attenuation distributions [2]. Maximum Likelihood reconstruction of Attenuation

✉ Alireza Kamali-Asl
a_kamali@sbu.ac.ir

1 Department of Medical Radiation Engineering, Shahid Beheshti University, Evin, Tehran 1983969411, Iran

2 Chronic Respiratory Diseases Research Center, National Research Institute of Tuberculosis and Lung Diseases (NRITLD), Shahid Beheshti University of Medical Sciences, Tehran, Iran

3 PET/CT and Cyclotron Center, Masih Daneshvari Hospital, Shahid Beheshti University of Medical Sciences, Tehran, Iran

4 Department of Medical Physics and Biomedical Engineering, Tehran University of Medical Sciences, Tehran, Iran

5 Research Center for Molecular and Cellular Imaging, Tehran University of Medical Sciences, Tehran, Iran

and Activity (MLAA) method was proposed to find both attenuation and attenuation-corrected activity maps at the same time using a constrained maximum likelihood (ML) framework [8]. Due to the non-uniqueness of the solution for ML framework, the cross-talk artifacts often appear on the estimated activity and attenuation maps where some activity features in the activity map, such as image noise, propagate into the attenuation map and vice versa. Since TOF-PET data contain information about attenuation factors, TOF information can suppress the cross-dependencies between activity and attenuation maps [9]. In fact, count statistics of emission data and time resolution are the most important parameters that underpin the efficiency of the simultaneous reconstruction approach. Defrise et al. [10] showed that TOF-PET emission data can be used to for determination of activity and attenuation distributions up to an unknown scaling factor. Moreover, even under ideal conditions, this factor is object-dependent and hence TOF-PET emission data does not completely define attenuation map.

Because emission tomography is an ill-posed problem, image reconstruction can benefit from the imposing a priori knowledge as a regularization constraint in particular within a Bayesian reconstruction framework. The prior probability distribution of the unknown image plays an important role in this framework. A common form of prior information can be obtained based on the spatial smoothness or piecewise spatial smoothness. These priors usually rely on intensity differences between individual pixels and force pixel values to be similar to neighbors. The main drawbacks of these priors are the need for a positivity constraint and difficulty of choosing the optimal parameters for prior (hyperparameter).

This study aims at improving the performance of MLAA algorithm using incorporation of histogram-based information and making a nearly segmented attenuation map to reduce the cross-talk on MLAA method. The proposed method utilizes a novel approach based on mixture models that make a more uniform attenuation map at each step of MLAA iteration beside the advantages of smoothing priors. The histogram-based mixture models use "pointwise" priors that have no neighbor interactions in contrast to smoothing priors and each voxel can be drawn to a cluster with its own local mean and some degree of "confidence" parameters. The parameters of mixture model prior on the proposed method are calculated simultaneously from a MAP procedure at the reconstruction step and the prior needs no positivity enforcement. Another advantage of the proposed method is that it produces a segmented attenuation map during the reconstruction that is efficient for resolving the scaling problem of emission-based methods or combing the proposed method with other attenuation map extraction methods on PET/MR system.

Materials and methods

The basic of emission-based method for attenuation correction

In TOF-PET, the mean of expected counts for line of response (LOR) i in such that two annihilation photons detected on the time difference of t, are denoted as follows:

$$\bar{g}_{it} = n_i \, e^{-\sum_k l_{ik}\mu_k} \sum_{j=1}^{J} c_{ijt} \, \lambda_j + n_i \, \bar{S}_{it} + \bar{r}_{it}, \tag{1}$$

where λ_j and μ_k are the activity and attenuation values at voxel j and k, respectively, j is the total number of voxels, c_{ijt} is the probability that an emission from voxel j is detected in LOR i in the absence of attenuation (system model), l_{ik} denotes the attenuation intersection length of LOR i with voxel k, $\bar{S}_{it}$ and $\bar{r}_{it}$ are the expected contribution of scatter and randoms, respectively, and n_i shows the normalization factor for each LOR. The activity and attenuation map can be found using the likelihood maxima:

$$L\big((\lambda, \mu)|g_{it}\big) = \sum_{it} g_{it} \, ln\bar{g}_{it} - \bar{g}_{it}, \tag{2}$$

where g_{it} is the measured count of detected coincidences for LOR i and TOF bin t. This likelihood function is not concave when λ and μ are treated as unknown distributions. MLAA algorithm uses the alternation updates of λ and μ which converge toward a local optimum [8]. However, it should be noted that, in transmission tomography, attempts at developing EM algorithm have not resulted in an updateable expression for likelihood increment at each iteration [11]. Also, it is shown that the complete variables do not disappear from the equations like emission tomography [12]. Hence, the use of a gradient-ascent algorithm is suggested, which directly maximizes likelihood function and due to the use of only regular projection/backprojection operators, its implementation would be similar to emission tomography [12].

Incorporation of priors

To suppress cross-talk and confine the solution space, some constraints such as range and local smoothness priors for activity or attenuation maps must be imposed on the reconstruction [6, 8]. Due to low counting rates and the limited acquisition time of PET data acquisition, usually the use of a smoothing prior removes the divergence in quantitative accuracy at higher iteration numbers and produces a smoother image in contrast to the same number of iterations to the MLEM approach. Our aim is to produce a more uniform attenuation map in such a

way that the attenuation histogram would be composed of a limited number of peaks to have a reduction in the number of unknown attenuation coefficients. Bayesian estimation, or Maximum a Posteriori (MAP) estimation is a statistical approach that can be used to incorporate prior information on the reconstruction. Based on the Bayes' theorem:

$$p(\lambda, \mu, \psi|g) = \frac{p(g|(\lambda, \mu))p((\lambda, \mu)|\psi)p(\psi)}{p(g)}, \tag{3}$$

where $p((\lambda, \mu, \psi)|g)$ is the joint posterior, $p(g|(\lambda, \mu))$ denotes the likelihood function (forward model of the imaging system), the term $p((\lambda, \mu)|\psi)$ shows the prior and depends on the parameters of ψ, and term $p(\psi)$ is known as hyperprior on ψ. Because the prior knowledge about attenuation distribution will only be applied in the attenuation map, so $p(\lambda)$ would be independent of ψ and $p((\lambda, \mu)|\psi) = p(\lambda)\, p(\mu|\psi)$. Based on the MAP principle, the final objective function would be:

$$\Phi_{\text{Total}}(\lambda, \mu, \psi) = \Phi_{\text{L}}(g|\lambda, \mu) + \Phi_{\text{p}}(\mu|\psi) + \Phi_{\text{HP}}(\psi), \tag{4}$$

where Φ_L, Φ_{p}, Φ_{HP} denote the objective functions corresponding to the logarithm of the likelihood, prior, and hyperprior terms, respectively. An iterative framework can be used to extract activity and attenuation maps and also prior parameters from this objective function. The alternating proposed algorithm can be summarized by the diagram in Fig. 1.

At each iteration, by holding μ at its current values, λ is updated and then while holding the most recent estimates of λ and ψ fixed, μ will be updated and finally updating the parameters ψ with the latest estimate of μ is performed. Based on this strategy, the general framework of MAP procedure can be written as:

$$\hat{\lambda}^{k+1} = \arg\max_{\lambda \geq 0} \left\{\Phi_{\text{L}}\left(g|(\lambda, \mu^k)\right) + \Phi_{\lambda}(\lambda)\right\}, \tag{5}$$

$$\hat{\mu}^{k+1} = \arg\max_{\mu \geq 0} \left\{\Phi_{\text{L}}\left(g|(\lambda^k, \mu)\right) + \Phi_{\text{p}}\left(\mu|\psi^k\right)\right\}, \tag{6}$$

$$\hat{\psi}^{k+1} = \arg\max_{\psi} \left\{\Phi_{\text{p}}\left(\mu^{k+1}|\psi\right) + \Phi_{\text{HP}}(\psi)\right\}. \tag{7}$$

It should be mentioned that $p(\lambda)$ and hyperprior pdf $p(\psi)$ are modeled as uniform without any loss of generality; hence, terms of $\Phi_{\lambda}(\lambda)$ and $\Phi_{\text{HP}}(\psi)$ can be dropped in the derivations.

Note that Eq. (5) leads to the same activity reconstruction problem on a PET system with known attenuation map. The activity map can be calculated by applying a single iteration of the Maximum Likelihood Exception Maximization (ML-EM) routine.

$$\lambda_i^{h+1} = \frac{\lambda_i^h}{\sum_{it}\left(c_{ijt}\, e^{-\sum_j l_{ij}\mu_j^h}\right)} \sum_{it}\left(\left(e^{-\sum_j l_{ij}\mu_j^h}\right) \frac{c_{ijt}\, y_{it}}{\sum_{i\zeta} a_i^h c_{i\zeta t}\lambda_\zeta^h + s_{it}}\right). \tag{8}$$

Equation (7) can be considered a parameter fitting to the latest estimate of μ. The histogram of attenuation map can be assumed to be comprised of several peaks such that each of them belongs to a particular tissue type such as air background, lung, soft tissue, and bone in the body. Thus, a finite mixture model comprising L component distributions can be defined as a prior (each component is indexed by a).

$$\Phi_{\text{p}}\left(\mu^{k+1}|\psi\right) = \sum_{j=1}^{J} \log\left(\sum_{a=1}^{L} \pi_a p(\mu_j|\theta_a)\right) \tag{9}$$

where θ_a, π_a are the parameters of density function for class a ($a = 1;\ldots; L$) and $p(\mu_j|\theta_a)$ shows the probability that attenuation coefficient of voxel j belongs to class a with the parameter θ_a. The parameter π_a can be viewed as mixing proportion of class a that shows the area under each peak $\left(\sum_{a=1}^{L} \pi_a = 1; a \geq 0\right)$. Based on this definition, it can be

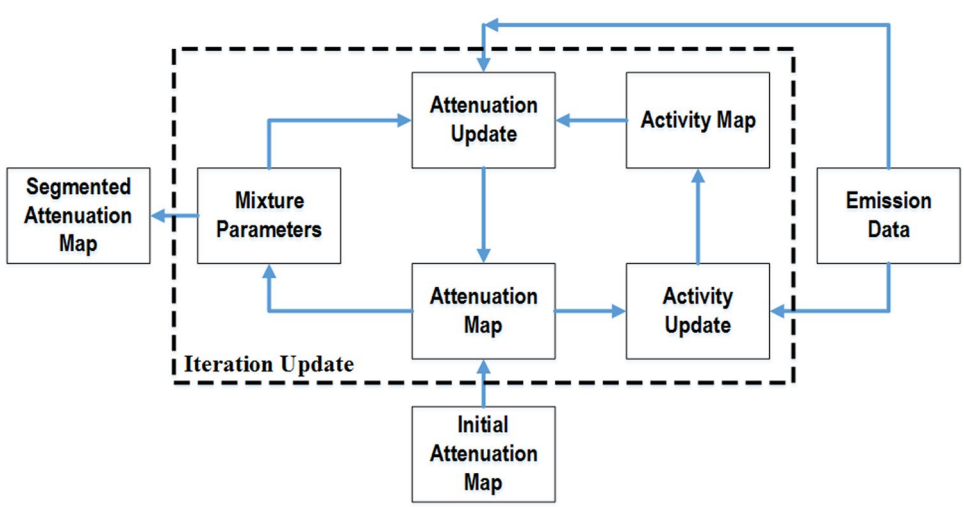

Fig. 1 Algorithm for joint estimation of activity and attenuation maps from measured emission TOF-PET data based on the mixture models prior

considered that the attenuation map histogram consists of L peaks corresponding to the different anatomical regions of attenuation map. The peak density function can be models as a Gaussian mixture models with parameters $\bar{\mu}_a, \sigma_a$ that are the mean and the standard deviation of the Gaussian functions for each class, respectively.

$$p\left(\mu_j|\theta_a = \bar{\mu}_a, \sigma_a\right) = \frac{1}{\sqrt{2\pi}\sigma_a} \exp\left(-\frac{1}{2}\left(\frac{\mu_j - \bar{\mu}_a}{\sigma_a}\right)^2\right). \tag{10}$$

Parameter Estimation from Eq. (7) is a mixture decomposition problem and there are some methods for optimizing it based on an efficient EM algorithm. Hathaway [13] proposed an alternative objective function based on the interpretation of EM algorithm for mixture distributions that leads to the same solution as EM steps for $\Phi_{\mathrm{p}}(\mu|\bar{\mu}, \sigma, \pi)$.

Let:

$$\Omega = \left\{ \left(\pi_1, \ldots, \pi_L, \bar{\mu}_1, \ldots, \bar{\mu}_L, \sigma_1, \ldots, \sigma_L\right): \sum_{a=1}^{L} \pi_a = 1 \; and \; \pi_a \geq 0, \; (\bar{\mu}_a, \sigma_a) \, \varepsilon \Omega_a \; for \; 1 \leq a \leq L \right\}$$
$$M = \left\{ W \varepsilon R^{LJ}; 0 \leq W_{aj} \leq 1, \; \sum_{a=1}^{L} W_{aj} = 1, \quad for \; 1 \leq a \leq L, \; 1 \leq j \leq J \right\} \tag{11}$$

where W_{aj} shows the probability of voxel j belongs to the class of a and hence W can be viewed as segmented attenuation map. The new objective function defined over $M \times \Omega$, as below:

$$\Phi_p^{\mathrm{hath}}(\mu|\, \bar{\mu}, \sigma, \pi, W) = -\sum_{j=1}^{J}\sum_{a=1}^{L}\left(W_{aj}\log W_{aj} + W_{aj}\log\frac{1}{\pi_a p_a(\mu_j|\bar{\mu}_a, \sigma_a)}\right) \tag{12}$$

where the first term shows the statistical uncertainty (negative of the sum of the entropies) and the second term can be viewed as a weighted distance function that shows a probabilistic measure of the distance between μ_j and subpopulation a. Using this alternative objective function simplifies ML estimation and derivations of the hyper parameters of mixture model prior and hence the parameters of histogram-based prior can be calculated by optimizing (Eq. 12) on a grouped coordinate descent update [14].

In this study, beside the mixture model prior, a Median root prior (MRP) was used to reduce the noise between neighbor voxels in the attenuation map to be locally monotonic. This smoothing prior is based on the assumption that inside a local neighborhood, there is no spatial difference between voxels values. No need for any tuning on the derivation of the energy function is its significant advantage. This penalty is based on the difference of voxel values against the local median and will be activated only if the attenuation map contains non-monotonic structures inside a local neighborhood and would be deactivated if the image is locally monotonic. Finally Eq. (5) can be rewritten as:

$$\hat{\mu}^{k+1} = \arg\max_{\mu \geq 0}\left\{\Phi_L\left(g|(\lambda^k, \mu)\right) + \alpha\, \Phi_{\mathrm{p}}^{\mathrm{hath}}\left(\mu|\psi^k\right) + \beta\left(-\sum_{j=1}^{J}\frac{\left(\mu_j - m_j\right)^2}{2m_j}\right)\right\} \tag{14}$$

where α and β adjust the strength of mixture model and MRP priors, respectively, and m_j denotes the median of voxels in the neighborhood centered at j. Equation (14) can be viewed as a gradient-ascent transmission tomography method and hence the attenuation map can be calculated using an iterative approach [12].

Experiments

The performance of the proposed approach using both simulated and experimental studies was investigated in comparison with MLAA algorithm. For simulations studies, the scanner geometry and specifications of the simulated PET system were similar to Siemens Biograph mCT PET/CT system [15]. The measured TOF data in mCT system are organized as sinogrmas, consisting of 400 radial bins, 168 angular bins, 109 direct planes and 13 TOF bins with effective time resolution of 580 ps. Since the proposed method (in general, any emission-based method) does not provide complete attenuation estimation for non-support activity regions, a background mask resulted from a few non-corrected activity reconstruction was used to confine the attenuation map reconstruction within body contour. For these experiments, the initial attenuation map was obtained by filling the background mask uniformly with tissue attenuation coefficient.

Results

Thorax numerical phantom

To investigate the general feasibility and accuracy of the proposed method for extraction of information about the attenuation from the emission (PET) data, TOF-PET data from a

numerical thorax phantom was used. The reconstruction was performed with a matrix size of 200 × 200 using 10 iterations and 20 subsets. Reconstructed activity and attenuation maps using the proposed method and TOF-MLAA method were shown in Fig. 2. Also, Fig. 3 shows the obtained segmented map from the proposed method for different tissue type classes.

The line profiles of the reconstructed attenuation maps using MLAA and proposed method were depicted on Fig. 4. A sense of the performance of the proposed method on the noise and cross-talk reduction can be revealed in the Fig. 5 which shows pixel by pixel difference between actual activity and attenuation images and reconstructed images using MLAA and proposed methods. The proposed method is successful on the cross-talk and noise reduction for reconstructed attenuation map.

Figure 6 shows the reconstructed activity and attenuation maps of the numerical thorax phantom after 3, 6, 10 and 20 iterations using proposed method. The reconstructed images does not show any sign of activity and attenuation cross-talks after 20 iterations for reconstructed maps using proposed method. Figure 7 illustrates the signal to noise ratio (SNR) at each global iteration for the reconstructed attenuation and activity maps using MLAA and proposed method of the thorax phantom. It can be concluded that improving the quality for attenuation map brings the activity image closer to the actual one.

Impact of system time resolution on the reconstructed attenuation map

To explore the limiting impact of system time resolution on performance of the proposed method, a Monte Carlo simulation study of NEMA IEC body phantom was utilized. The Geant4 Application for Emission Tomography (GATE) [16] code was used to generate the simulation data of IEC phantom at different time resolutions of 100 and 580 ps in the absence of noise and dead time. According to the NEMA NU 2-2007 standard [17], this phantom is recommended for use in the evaluation of reconstructed image quality in whole-body PET imaging [18]. The NEMA IEC phantom comprises 6 hollow glass spheres with various sizes (inner diameters of 37, 28, 22, 17, 13, and 10 mm) into the torso-shaped fillable compartment with cavity of 9.7 L and interior length

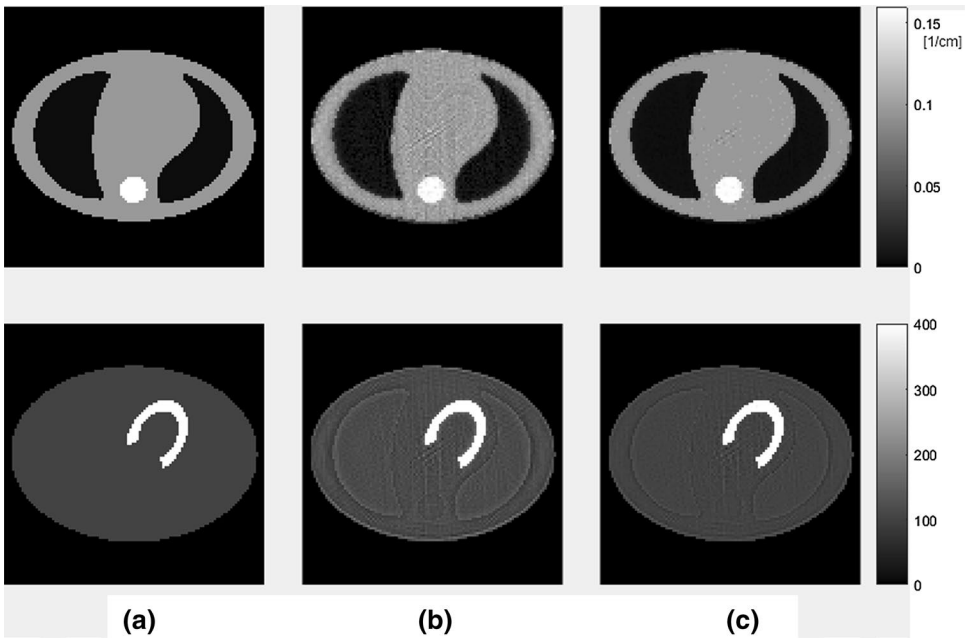

Fig. 2 Attenuation (top) and activity (bottom) maps of numerical phantom. **a** Actual, **b** reconstructed images using MLAA method and **c** proposed method

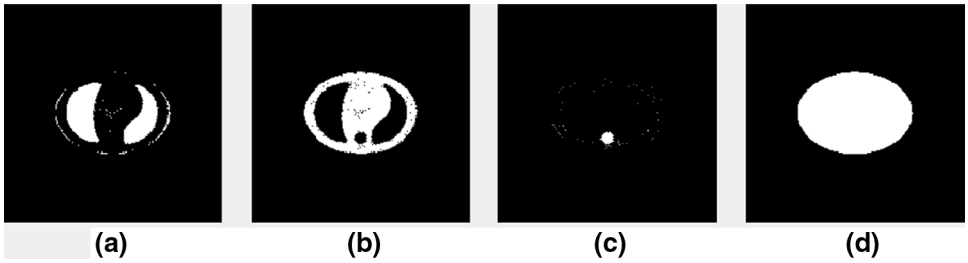

Fig. 3 The estimated segmentation map (W_{aj}) for three classes of numerical phantom **a** $a=1$, **b** $a=2$, **c** $a=3$ and **d** $\sum W_a$

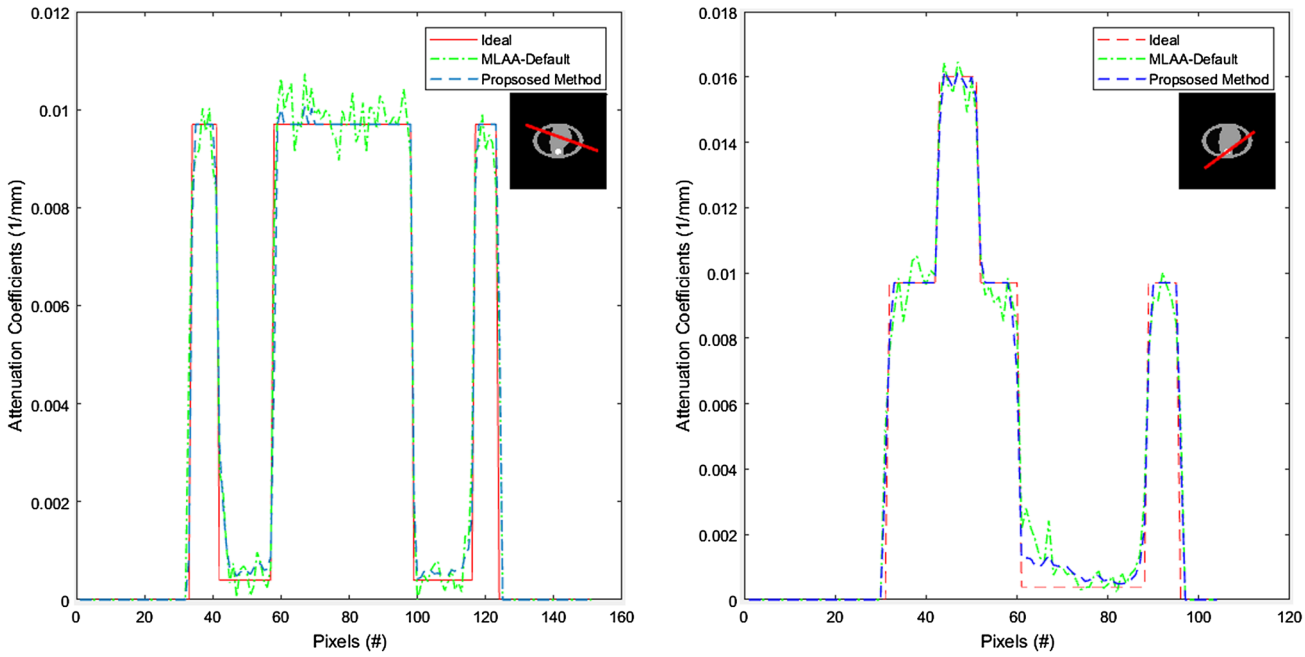

Fig. 4 Line profiles through the actual and reconstructed attenuation maps of different methods for numerical thorax phantom

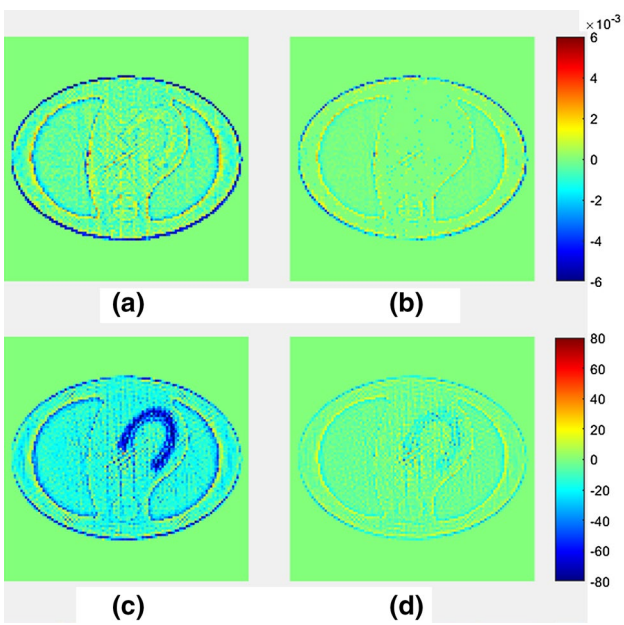

Fig. 5 **a, c** The pixel by pixel difference maps between actual and reconstructed images using MLAA and **b, d** the difference maps between actual and reconstructed images using the proposed method of numerical phantom for reconstruction with 20 subsets and 10 iterations. The top row images belong to the attenuation distributions, while the bottom images show activity differences

of 180 mm. Additionally, a cylindrical insert with density of 0.3 ± 0.1 g ml^{-1} was positioned in the center of the phantom to model patient lung tissue. The four smaller spheres are filled with FDG as hot sources, while the larger ones are filled with non-radioactive water as cold regions. The activity concentration in the hot regions was about 4 times that of the background. The simulations were performed for 300 s with the activity of 530 kBq/ml. The actual and reconstructed images using MLAA and proposed method at different time resolution after reconstruction with 10 iterations on the list-mode format were shown on Fig. 8. In addition, Fig. 9 shows the line profiles of the reconstructed attenuation maps. The proposed method was successful in estimating a roughly identical map with the actual attenuation map on the time resolution of 100 ps (ideal system). However, there is some underestimation for estimation of attenuation coefficient of lung region than to the actual one, but the problem of underestimation of attenuation coefficients especially for body region in MLAA method was reduced. The estimated segmentation map of reconstructed attenuation map for two classes of simulated NEMA IEC phantom were shown in Fig. 10. The segmentation procedure is well-done at time resolution of 100 ps without creating too many misclassified voxels.

Performance on phantom scan

An implementation of proposed method has been applied to the emission data of a NEMA IEC body phantom scan that have been acquired on a Siemens Biograph mCT system for 5 min scan and hot to background ratio of 2. The phantom 0was located in the center of the FOV

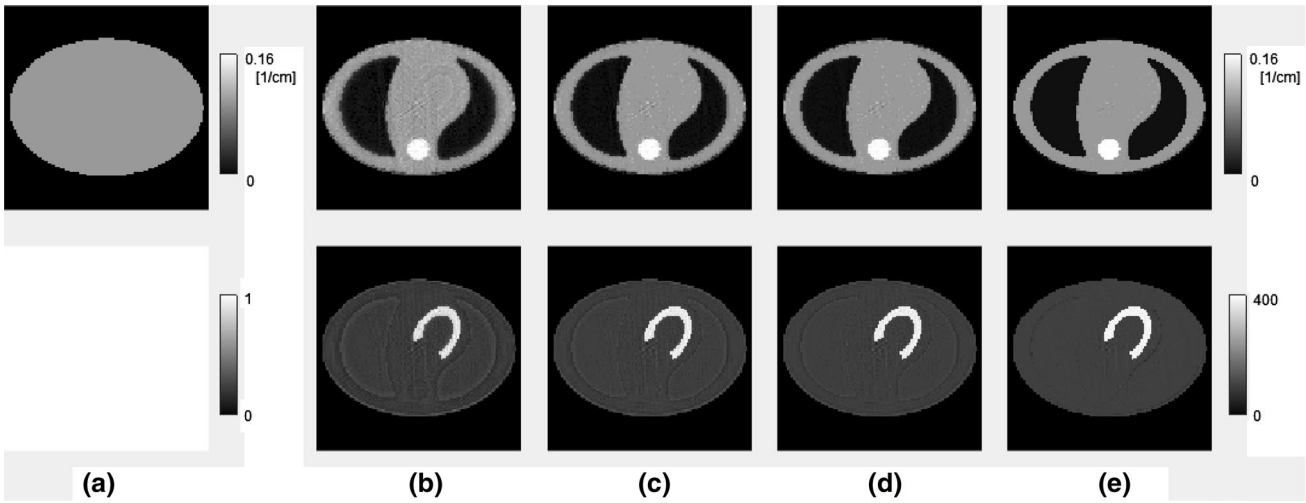

Fig. 6 **a** Initial and reconstructed attenuation (top row) and activity maps (bottom row) images after 20 subsets and **b** 3, **c** 6, **d** 10 and **e** 20 iterations on system time resolution of 580 ps

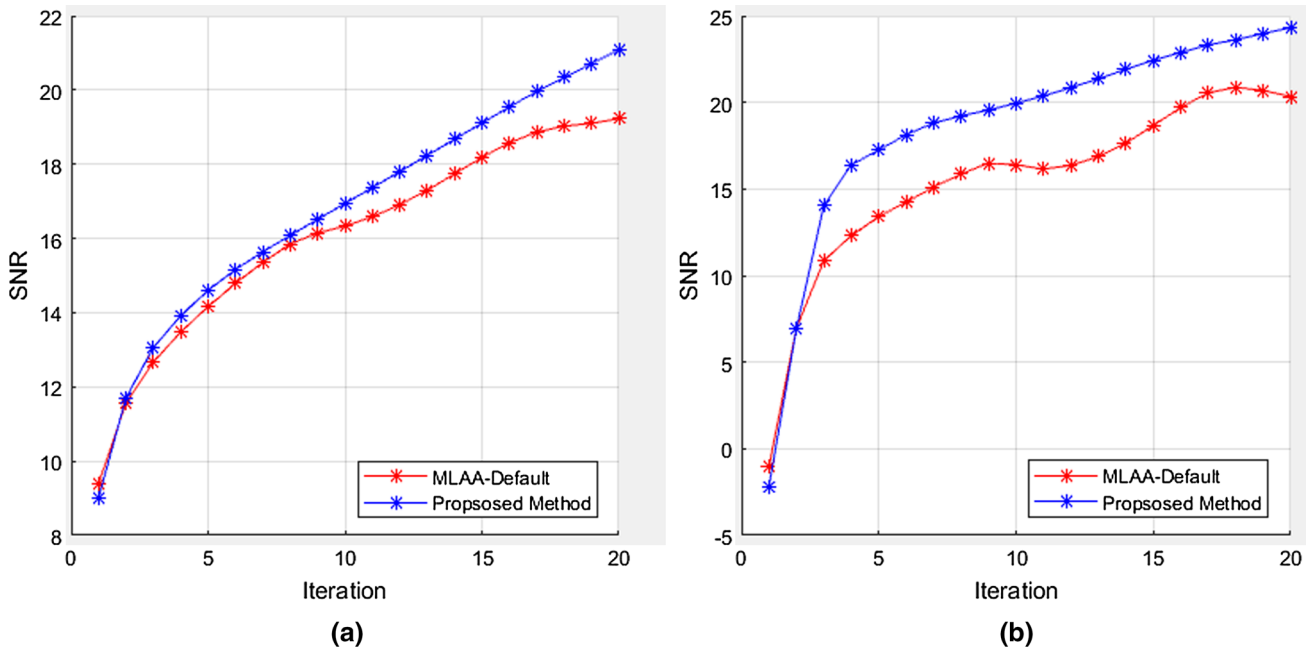

Fig. 7 The signal to noise ratio (SNR) of the estimated maps vs. the global iteration number of the thorax phantom for reconstructed **a** attenuation and **b** activity images using different methods

and the reconstruction performed with a matrix size of $200 \times 200 \times 109$ and slice thickness of 2.027 using 5 iteration of 20 subsets. The scatter components and decay correction factor were not considered on the reconstruction. However in this study, there is no enforcement for adding the bed attenuation coefficients in the attenuation map, but a bed attenuation template calculated by a transmission scan using CT can be used to be accounted in the attenuation map during reconstruction. The CT-based corrected activity and the CT-based attenuation maps together with the reconstructed activity and attenuation maps using the proposed method for a different transaxial plane are shown in Fig. 11. Although the proposed method has been able to distinguish the body attenuating materials from the central cavity in the reconstructed attenuation map, there is some excess attenuation around the edge of phantom. Also, slight activity was observed within the central cavity of activity images of the phantom. The mentioned

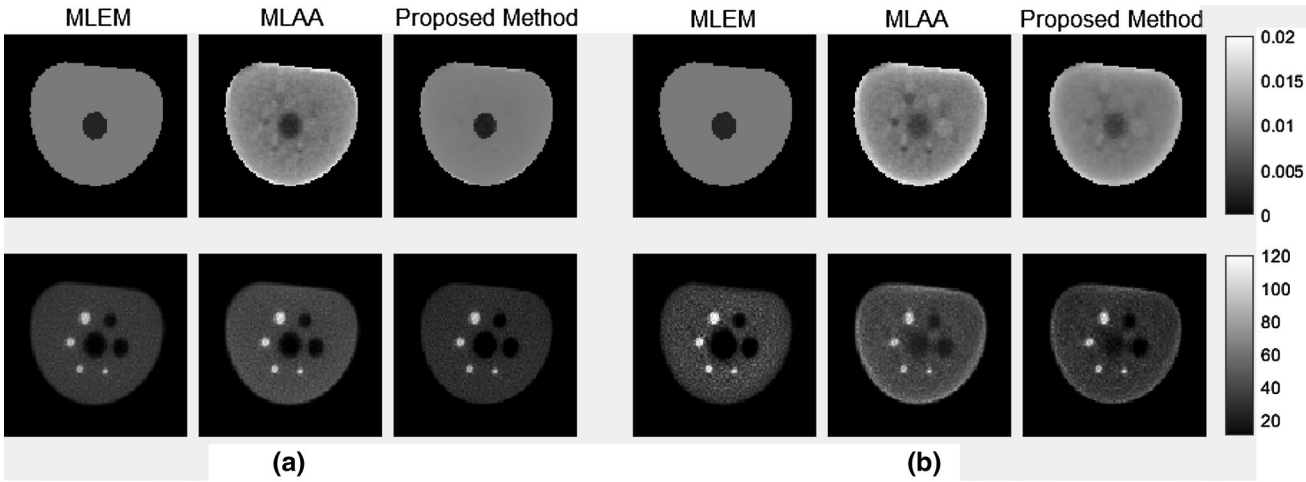

Fig. 8 MLEM reconstructed activity using known attenuation map and reconstructed activity and attenuation maps of simulated NEMA IEC phantom using MLAA and proposed methods at time resolutions of **a** 100 ps and **b** 580 ps. For each section, columns from left to right depict reconstructed attenuation (top) and activity (bottom) reconstructed maps using MLEM, MLAA and proposed methods, respectively. The images are magnified by factor 2

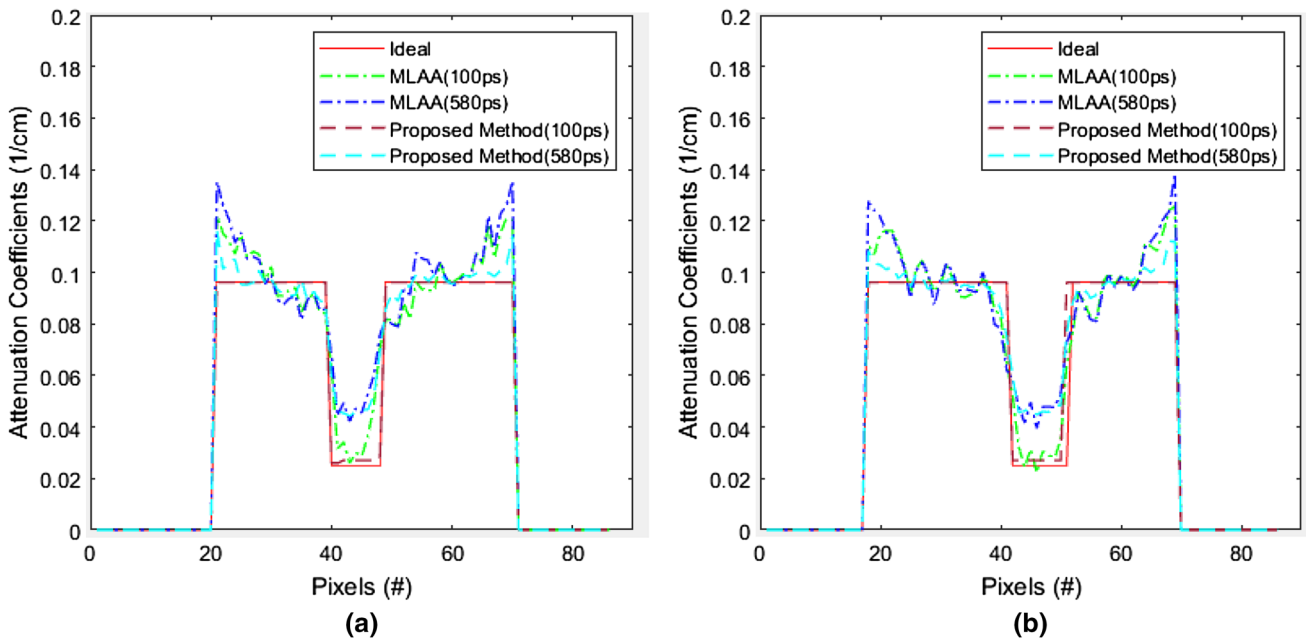

Fig. 9 The profiles of reconstructed attenuation map using MLAA and proposed methods at different time resolutions of 100 and 580 ps compared to their actual profiles for NEMA NU 2-1994 phantom

problems in the reconstructed images may be due to the lack of scatter correction for this phantom. The overestimation of the object boundary due to the inaccurate estimation of background mask can be another possible reason. Figure 12 shows the W complete data set of this phantom in different views. The model-based scatter correction (MBSC) approach [19] can be used for estimation of scatter contributions. To do this, it is necessary to use an iterative approach such that the scatter contribution estimation is updated for current estimation of attenuation and activity images. Although model-based scatter correction techniques accurately estimate the scatter components, the computational cost of the proposed method increases.

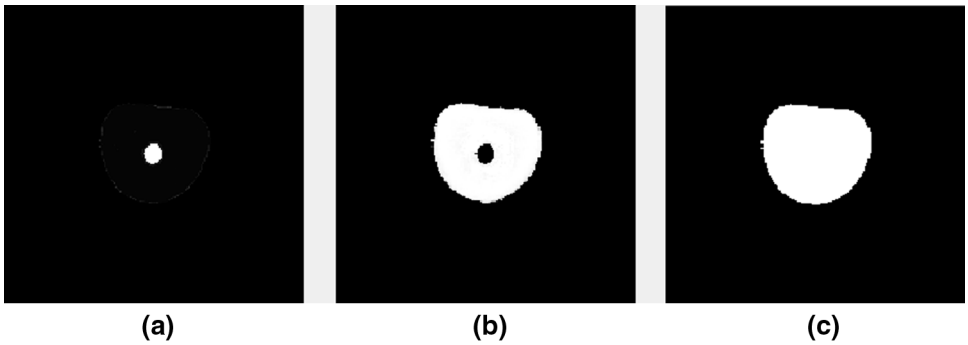

Fig. 10 The estimated segmentation map (W_{aj}) for different classes of simulated NEMA IEC phantom with system time resolution of 100 ps on the classes of **a** $a=1$, **b** $a=2$ and **c** $\sum W_a$

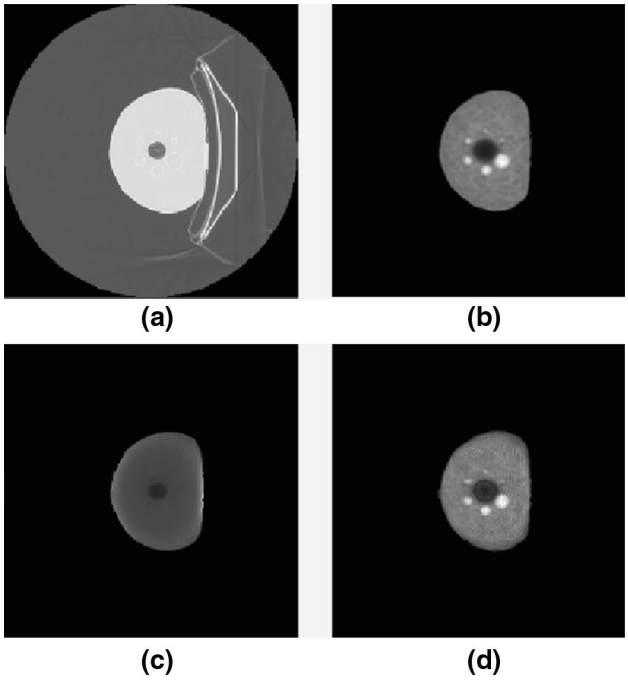

Fig. 11 **a** CT-based attenuation map, **b** MLEM activity reconstruction using CT-based attenuation map, **c, d** attenuation and activity reconstructed maps using proposed method on the 3D NEMA IEC phantom

Discussions

In this study, a novel joint-MAP reconstruction/segmentation method was presented for estimating the attenuation map from TOF-PET emission data by incorporating histogram information. Beside adding a new prior to MLAA method that assumes a clustered intensity histogram in the attenuating object and enforcing of positivity in MAP method, the proposed method can segment attenuation map during the reconstruction. Use of Mixture model prior can significantly reduce noise and cross-talk artifacts on the reconstructed images. In the proposed method, the strength of the mixture model at each iteration is controlled by parameter α. With reduction in this parameter, the algorithm leads to the original MLAA ($\alpha = 0$), while a high value of it converts the method to a segmentation process for the attenuation map at each iteration ($\alpha \geq 1$) [14]. In other words, this parameter controls how much the histogram values are close to the multi Gaussian functions. Because the proposed method makes the complete data set W beside the attenuation map at each iteration and it acts as a segmentation result of the attenuation map, so the low value of α is preferred. In addition, in this case the mean of the attenuation coefficients gets close to the expected values of MLAA.

One of the interesting features of the proposed method is that parameter L (the number of classes in the mixture model) can be fixed to 3 or 4 classes (similar to the MR-based segmentation method) or be chosen as a patient-dependent parameter. There are some methods to choose this parameter based on image context [20, 21]. It has been observed that the increment in this parameter may have an effect on the reduction in the misclassified voxels, although the processing time would increase.

The attenuation coefficients on the TOF-PET system can be determined from emission data up to a constant scaling factor. It is suggested for determining this additive constant, the known attenuation coefficient is imposed to a segmented portion (a region containing (mostly) tissue) of the attenuation image [6, 10]. Hence, the segmentation of the attenuation map for resolving the scaling problem seems to be necessary. However, emission-based methods usually produce a noisy attenuation map due to the noise and nonstationary statistics of photon and hence more sophisticated segmentation algorithms may be needed. The proposed method makes an attenuation map in such a way that its histogram is composed of a limited number of Gaussian functions with a certain mean and standard deviation for each peak. Hence, the complexity of scaling problem for estimated attenuation coefficients is reduced on the proposed method and it can be solved through some different ways [22–25]. Also, because the complete data set W makes a segmented attenuation map, a similar method of current commercial systems can be

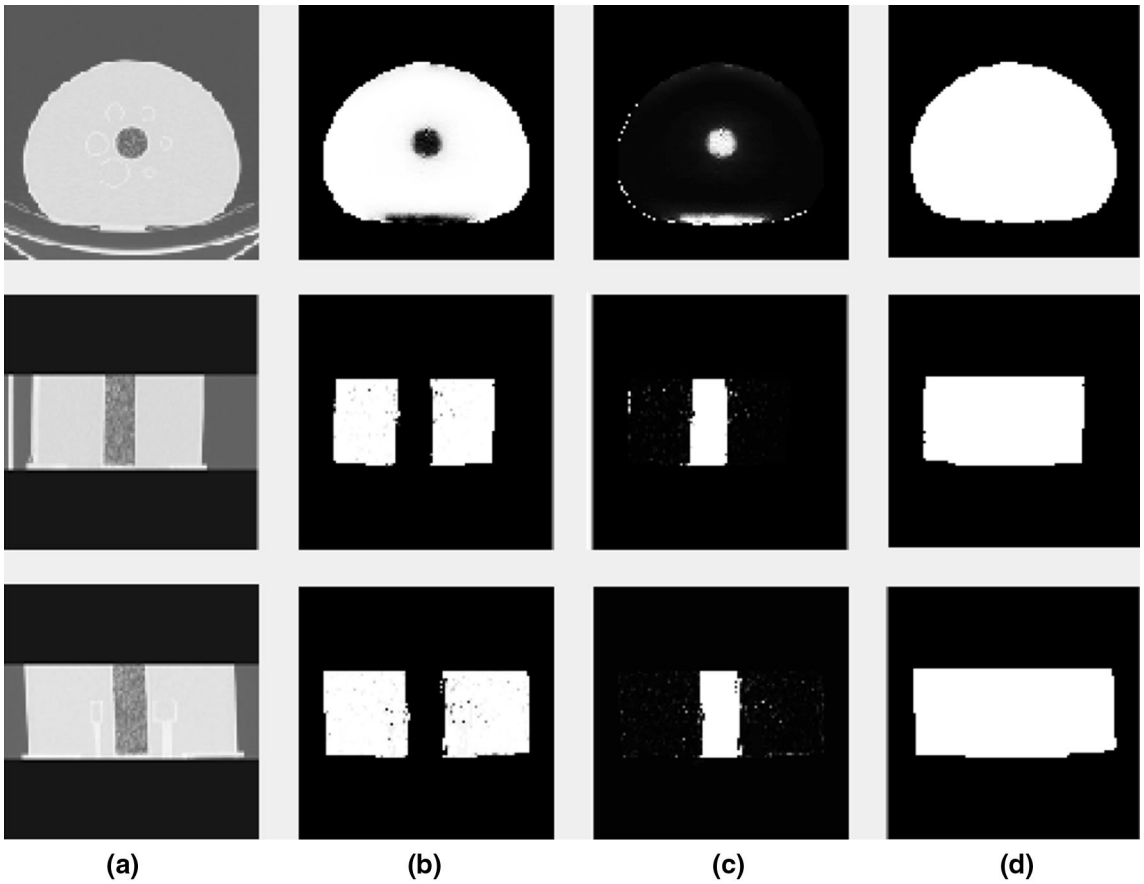

Fig. 12 **a** CT-based reference attenuation and **b**–**d** reconstructed segmentation maps (complete data set) for two classes of NEMA IEC phantom **b** $a=1$, **c** $a=2$ and **d** $\sum W_a$.(from up to down: transverse, coronal, and sagittal transection)

used, too. The predefined attenuation coefficients can be assigned to each segment using automatic methods based on the features of segments or by a manual method (an expert user). Another method is to fix the average of the Gaussian mixtures in the proposed method. In this way, the mixture decomposition step only estimates two other parameters (σ_a, π_a) at each iteration and the attenuation coefficients are assigned automatically to each segment.

The reconstruction using emission data needs computations of the activity and attenuation distributions as well as hyper parameters over an iterative approach, which leads to a computational burden. To overcome this problem, a graphic hardware acceleration can be utilized to speed up the different steps of the proposed method. Further simulation studies modeling even more realistic complex phantoms and clinical cases as well as multi-bed-position patient setups are required to further investigate the robustness of the method. Moreover, the use of other smoothing priors for the clinical case and combining the proposed method with other methods should be investigated.

Conclusions

We proposed a method that reconstructs patient-specific attenuation maps out of emission data to be used for the PET reconstruction of future PET/MR investigations. It is based on the clustering modeling of attenuation map histogram that allows direct classification of different anatomical regions of attenuation map. The proposed method offers similar correction accuracy as offered by the MR-based attenuation correction technique with sufficient reliability, when no MR image is used. The slow convergence of the proposed method is an impediment to the efficient application of it for clinical cases. Next stage will be devoted to the speeding the attenuation map estimation process. We believe that this method is promising, and it may provide an alternative to other attenuation map extraction techniques for quantitative PET imaging on PET/MR system. The method can be particularly appropriate for new systems with improved time resolution.

References

1. Akbarzadeh A, Ay MR, Ahmadian A, Alam NR, Zaidi H. MRI-guided attenuation correction in whole-body PET/MR: assessment of the effect of bone attenuation. Ann Nucl Med. 2013;27(2):152 – 62.
2. Keereman V, Mollet P, Berker Y, Schulz V, Vandenberghe S. Challenges and current methods for attenuation correction in PET/MR. Magn Reson Mater Phys Biol Med. 2013;26(1):81–98.
3. Hofmann M, Steinke F, Scheel V, Charpiat G, Farquhar J, Aschoff P, et al. MRI-based attenuation correction for PET/MRI: a novel approach combining pattern recognition and atlas registration. J Nucl Med. 2008;49(11):1875–83.
4. Khateri P, Rad HS, Jafari AH, Ay MR. A novel segmentation approach for implementation of MRAC in head PET/MRI employing Short-TE MRI and 2-point Dixon method in a fuzzy C-means framework. Nucl Instrum Methods Phys Res Sect A Accel Spectrom Detect Assoc Equip. 2014;734:pp. 171–4.
5. Khateri P, Rad HS, Jafari AH, Kazerooni AF, Akbarzadeh A, Moghadam MS, et al. Generation of a four-class attenuation map for MRI-based attenuation correction of PET data in the head area using a novel combination of STE/Dixon-MRI and FCM clustering. Mol Imaging Biol. 2015;17(6):884 – 92.
6. Rezaei A, Defrise M, Bal G, Michel C, Conti M, Watson C, et al. Simultaneous reconstruction of activity and attenuation in time-of-flight PET. IEEE Trans Med Imaging. 2012;31(12):2224–33.
7. Xu M, Cutler P, Luk W. Adaptive, segmented attenuation correction for whole-body PET imaging. IEEE Trans Nucl Sci. 1996;43(1):331–6.
8. Nuyts J, Dupont P, Stroobants S, Benninck R, Mortelmans L, Suetens P. Simultaneous maximum a posteriori reconstruction of attenuation and activity distributions from emission sinograms. IEEE Trans Med Imaging. 1999;18(5):393–403.
9. Conti M. Why is TOF PET reconstruction a more robust method in the presence of inconsistent data? Phys Med Biol. 2010;56(1):155.
10. Defrise M, Rezaei A, Nuyts J. Time-of-flight PET data determine the attenuation sinogram up to a constant. Phys Med Biol. 2012;57(4):885.
11. Mumcuoglu EU, Leahy R, Cherry SR, Zhou Z. Fast gradient-based methods for Bayesian reconstruction of transmission and emission PET images. IEEE Trans Med Imaging. 1994;13(4):687–701.
12. Nuyts J, De Man B, Dupont P, Defrise M, Suetens P, Mortelmans L. Iterative reconstruction for helical CT: a simulation study. Phys Med Biol. 1998;43(4):729.
13. Hathaway RJ. Another interpretation of the EM algorithm for mixture distributions. Stat Probab Lett. 1986;4(2):53 – 6.
14. Hsiao T, Rangarajan A, Gindi G. Joint-MAP Bayesian tomographic reconstruction with a gamma-mixture prior. IEEE Trans Image Process. 2002;11(12):1466–77.
15. Jakoby B, Bercier Y, Conti M, Casey M, Bendriem B, Townsend D. Physical and clinical performance of the mCT time-of-flight PET/CT scanner. Phys Med Biol. 2011;56(8):2375.
16. Jan S, Santin G, Strul D, Staelens S, Assie K, Autret D, et al. GATE: a simulation toolkit for PET and SPECT. Phys Med Biol. 2004;49(19):4543.
17. Goertzen AL, Bao Q, Bergeron M, Blankemeyer E, Blinder S, Cañadas M, et al. NEMA NU 4-2008 comparison of preclinical PET imaging systems. J Nucl Med. 2012;53(8):1300–9.
18. Watson CC, Casey ME, Eriksson L, Mulnix T, Adams D, Bendriem B. NEMA NU 2 performance tests for scanners with intrinsic radioactivity. J Nucl Med. 2004;45(5):822–6.
19. Ollinger JM. Model-based scatter correction for fully 3D PET. Phys Med Biol. 1996;41(1):153.
20. Liang Z, Jaszczak RJ, Coleman RE. Parameter estimation of finite mixtures using the EM algorithm and information criteria with application to medical image processing. IEEE Trans Nucl Sci. 1992;39(4):1126–33.
21. Richardson S, Green PJ. On Bayesian analysis of mixtures with an unknown number of components (with discussion). J R Stat Soc Ser B (Stat Methodol). 1997;59(4):731 – 92.
22. Boellaard R, Hofman M, Hoekstra O, Lammertsma A. Accurate PET/MR quantification using time of flight MLAA image reconstruction. Mol Imaging Biol. 2014;16(4):469 – 77.
23. Berker Y, Kiessling F, Schulz V. Scattered PET data for attenuation-map reconstruction in PET/MRI. Med Phys. 2014;41(10):102502.
24. Hemmati H, Kamali-Asl A, Ay M, Ghafarian P. Compton scatter tomography in TOF-PET. Phys Med Biol. 2017;62(19):7641.
25. Rothfuss H, Panin V, Moor A, Young J, Hong I, Michel C, et al. LSO background radiation as a transmission source using time of flight. Phys Med Biol. 2014;59(18):5483.